Electronic supplementary information

Plasmon-enabled N_2 photofixation on partially reduced Ti_3C_2 MXene

Binbin Chang,[a] Yanzhen Guo,[c] Donghai Wu,[c] Li Li,[a] Jianfang Wang*[b] and Baocheng Yang*[c]*

[a]Shanghai Key Laboratory of Green Chemistry and Chemical Processes, School of Chemistry and Molecular Engineering, East China Normal University, Shanghai 200241, China
[b]Department of Physics, The Chinese University of Hong Kong, Shatin, Hong Kong SAR, China
[c]Henan Provincial Key Laboratory of Nanocomposites and Applications, Institute of Nanostructured Functional Materials, Huanghe Science and Technology College, Zhengzhou 450006, China

Experimental

Preparation of the layered Ti_3C_2 MXene and partially reduced layered Ti_3C_2 MXene

The synthesis of the layered Ti_3C_2 was conducted according to the reported method.[1] Typically, 1 g of the prepared Ti_3AlC_2 powder (200 mesh) was dispersed in 10 mL of 40 wt% HF acid under magnetic stirring at 35 °C for 24 h. The resultant suspension was washed with deionized water by centrifugation until the pH value became near 7. The obtained wet Ti_3C_2 powder was dried in a vacuum oven at 60 °C overnight. To reduce Ti_3C_2, 0.5 g of the as-obtained dry Ti_3C_2 powder was heat-treated at 200 °C in a H_2 atmosphere (5 vol% in N_2) for 6 h to prepare the partially reduced layered Ti_3C_2 MXene, which was denoted as r-Ti_3C_2.

Preparation of the Au nanospheres

The citrate-capped Au nanospheres were prepared according to a previously reported method with slight modifications.[2] Typically, 50 mL of $HAuCl_4$ solution (0.25 mM) was added in a 100-mL round-bottom flask. The solution was brought to boiling under stirring. 2.0 mL of sodium citrate solution (1 wt%) was then added. The reaction mixture was kept at the boiling

temperature under stirring for 30 min. The solution finally became wine red, suggesting the production of Au nanospheres. Through the variation of the sodium citrate amount in the solution, Au nanospheres with different sizes were synthesized. Specifically, 1.15, 1.0 and 2.0 mL of the sodium citrate solution gave Au nanospheres of 13, 16 and 19 nm in diameter, respectively.

The Au nanospheres coated with cetyltrimethylammonium bromide (CTAB) were prepared in aqueous solutions according to a previously reported seed-mediated growth method with slight modifications.[3] Briefly, for the preparation of the seed solution, 0.25 mL of $HAuCl_4$ solution (0.01 M) was added into 9.75 mL of CTAB solution (0.1 M), followed by the rapid injection of a freshly prepared, ice-cold $NaBH_4$ solution (0.01 M, 0.6 mL) under vigorous stirring. The resultant solution was placed in an oven at 30 °C and kept undisturbed for 4 h. 0.25 mL of the seed solution was rapidly injected into a growth solution composed of CTAB (0.1 M, 9.75 mL), water (190 mL), $HAuCl_4$ (0.01 M, 4 mL), and ascorbic acid (0.1 M, 15 mL). The reaction mixture was gently shaken for 30 s and then left undisturbed overnight at 30 °C. The resultant Au nanospheres were centrifuged and washed twice with water and finally re-dispersed into water for further use.

Synthesis of r-Ti_3C_2/Au and Ti_3C_2/Au

The sandwich-like r-Ti_3C_2/Au nanostructures were prepared by a simple solvent-driven method. Briefly, to drive the citrate-capped Au nanospheres into the interlayer space of the layered r-Ti_3C_2, 0.1 g of the r-Ti_3C_2 powder and 10 mL of water were mixed and sonicated for 20 min under flowing Ar. A pre-calculated volume of the citrate-capped Au nanosphere solution was then added. After the mixture was continuously sonicated for 10 min, H_2O was removed by rotary evaporation at 45 °C. The obtained powder was further dried in a vacuum oven at 60 °C for 6 h to get the final product, which was denoted as r-Ti_3C_2/Au. The Ti_3C_2/Au sample was prepared following the same procedure.

In addition, the r-Ti_3C_2/edge-Au sample was obtained by replacing the citrate-capped Au nanospheres with the CTAB-capped ones in the above procedure.

Characterization

X-ray diffraction (XRD) patterns were recorded on a Bruker D8 diffractometer using Cu Kα radiation (λ = 0.15418 nm) as the X-ray source. The scanning electron microscopy (SEM) images were acquired on an FEI Quanta 250 FEG microscope. Transmission electron microscopy (TEM) imaging was performed on an FEI Tecnai G2 20 microscope operated at 200 kV. The diffuse-reflectance absorption spectra were measured on a Japan U-4100 ultraviolet/visible/near-infrared spectrophotometer equipped with an integrating sphere accessory using $BaSO_4$ as the reference. The extinction spectra of the Au nanospheres and the absorption spectra for the determination of NH_3 were measured on the same spectrophotometer. The X-ray photoelectron spectroscopy (XPS) measurements were performed on an Escalab 250 Xi system (Thermo Fisher Scientific) with Al Kα as the X-ray source for excitation. The low-temperature electron paramagnetic resonance (EPR) spectra were acquired on a Bruker E500 EPR spectrometer at 77 K. N_2 temperature-programmed desorption (TPD) analysis was performed in a quartz reactor using a thermal conductivity detector. *In situ* diffuse-reflectance infrared Fourier transform spectroscopy (DRIFTS) was conducted on a Nicolet iS50 FT-IR spectrometer with a home-designed reaction cell. The Au atomic ratios in the catalyst samples were determined by inductively coupled plasma mass spectrometry (ICP-MS, Thermo Fisher). ^{1}H NMR spectra were measured on a Bruker Avance III spectrometer.

Nitrogen photofixation reaction

The N_2 photofixation reactions were carried out in a 100-mL quartz reactor with an opening of 5.6 cm in diameter under N_2 atmosphere at room temperature. In a typical reaction, 80 mg of the photocatalyst and 50 mL of water were added into the reactor. The mixture solution was sonicated for 10 min to achieve uniform dispersion and then bubbled with ultrapure N_2 at a flow rate of 100 mL min^{-1} for 30 min to remove dissolved air. The reactor was subsequently illuminated with a 300-W Xe lamp (PLS-SXE300C, Beijing Perfectlight Technology) and bubbled with N_2 at a flow rate of 50 mL min^{-1} under continuous stirring. An aliquot of the reaction solution (3.0 mL) was taken out at regular intervals using a syringe. The collected aliquots were centrifuged to remove the photocatalyst. The concentrations of NH_3 in the supernatant at different illumination durations were determined by Nessler's method. Typically, the supernatant solution (0.5 mL) was first diluted with H_2O (2 mL), followed by the addition of potassium sodium tartrate (0.2 M, 0.25 mL) and Nessler's reagent (0.09 M K_2HgI_4 in a 2.5 M

KOH aqueous solution, 0.25 mL). The solution was mixed thoroughly and left for 20 min. The produced NH_3 can react with iodide and mercury ions under alkaline conditions according to the reaction below[4]

$$2[HgI_4]^{2-} + NH_3 + 3OH^- \rightarrow Hg_2ONH_2I + 7I^- + 2H_2O \quad (1)$$

The NH_4^+ concentration was calculated by measuring the absorbance at 420 nm according to a pre-established calibration curve on an ultraviolet/visible/near-infrared spectrophotometer. Each photocatalytic N_2 fixation experiment, including the control experiments, was repeated three times under the same conditions. The average amount of the produced NH_4^+ and the standard deviation were calculated.

$^{15}N_2$ isotope labelling experiment

The $^{15}N_2$ isotope labelling experiments were performed to further verify the origin of the produced NH_3. In a typical experiment, 50 mL of water and 80 mg of the photocatalyst were added in the reactor. The reactor was sealed when $^{15}N_2$ was used as the feed gas. Before the supply of $^{15}N_2$, the reaction system was sequentially vacuumed, blown with Ar, and vacuumed again. The remaining illumination steps were the same as in the above regular photocatalytic reactions. After the reaction was completed, the reaction solution was collected and acidified to pH = 2.0 with HCl. Dimethyl sulfoxide-d6 (DMSO-d6, 0.3 mL) was then added to the solution (0.2 mL) for ^1H NMR measurements.

Apparent quantum efficiency measurements

For the measurement of the apparent quantum efficiencies (AQEs), the N_2 photofixation reactions were performed under monochromatic light using appropriate bandpass filters at different wavelengths (380, 420, 450, 475, 500, 520, 550, 578, 600, 650 and 700 nm, full widths at half maximum for all: 20 nm, Beijing MerryChange Technology). The corresponding power intensities were measured using an optical power meter (Molectron POWER MAX 5200). The AQEs under different monochromatic light were calculated according to the following equation

$$AQE\ (\%) = \frac{N_{\text{reacted}}}{N_{\text{incident}}} \times 100\% = \frac{3N_{NH_3}}{N_{\text{incident}}} \times 100\% = \frac{3n_{\text{NH}_3} \times N_{\text{A}}}{(W \times A \times t)/(hv)} \times 100\% \quad (2)$$

where N_{reacted}, N_{incident} and N_{NH_3} represent the numbers of the reacted electrons, the incident photons and the generated NH_3 molecules, respectively, W, A and t respectively denote the light

intensity, illumination area and illumination time, v is the light frequency, h is Planck's constant, and N_A is Avogadro's constant.

Solar-to-ammonia conversion efficiency measurements

To determine the solar-to-ammonia conversion efficiency (SACE), the photocatalytic N_2 fixation reactions were carried out in a sealed reactor under simulated AM1.5G light illumination. Typically, 200 mg of the photocatalyst and 50 mL of water were added into the reactor. The reaction system was vacuumed and blown with N_2 repeatedly several times to drive out the dissolved air completely and then sealed with a rubber plug. To make sure that the reaction system was filled with N_2, it was further bubbled for another 1 h with a N_2-filled balloon. After the reaction solution was subjected under the simulated AM1.5G light illumination for 1 h, the produced ammonia amount was determined using Nessler's method. In addition, the evolved gases were also measured on a gas chromatograph (CEAULIGHT GC-7900, TCD detector, Ar carrier gas). The photocatalytic reaction was repeated three times.

The SACE was calculated based on the equation below

$$\text{SACE} = \frac{\left[\Delta G^0 \; for \; NH_3 \; generation \; (J \; mol^{-1})\right] \times [evolved \; NH_3 \; (mol)]}{[total \; input \; light \; power \; (W)] \; \times [reaction \; time \; (s)]} \quad (3)$$

In the above equation, the ΔG^0 value for NH_3 generation is 339 kJ mol^{-1}. The overall illumination intensity of the AM1.5G light source was 100 mW cm^{-2} and the illumination area was 24.62 cm^2.

Electrochemical measurements

To prepare the working electrode, the catalyst was first dispersed in an ethanolic solution of Nafion (5.0 vol%) to form an ink (10 mg mL^{-1}). The resultant dispersion (0.2 mL) was then dip-coated onto an indium tin oxide (ITO)-coated glass electrode with a coated area of 1 cm^2 and allowed to dry in a vacuum oven overnight at room temperature. The photocurrent and electrochemical impedance spectroscopy (EIS) measurements were conducted on an electrochemical workstation (CHI 760E, Shanghai Chenhua) in a three-electrode system with an electrolyte solution of 0.5 M Na_2SO_4, using Pt foil as the counter electrode, the standard Ag/AgCl electrode as the reference electrode, and the ITO substrate as the working electrode.

Density functional theory calculations

All density functional theory (DFT) calculations were carried out using Vienna *Ab Initio* Simulation Package (VASP). The Perdew-Burke-Ernzerhof (PBE) functional within the generalized gradient approximation (GGA) was selected as the exchange correlation functional. The dispersion-corrected DFT-D3 scheme was employed to account for the van der Waals interaction.[5] The projector augmented wave potential was used with a plane-wave cutoff energy of 500 eV. All atoms were fully relaxed until the force on each atom was less than 0.01 eV $Å^{-1}$ and the convergence criterion of the total energy was set to be 10^{-5} eV. The Brillouin zone was sampled with a 3 × 3 × 1 Monkhorst–Pack mesh. A vacuum spacing of 15 Å was set to avoid the interaction between two neighboring images.

The adsorption energy (E_{ads}) of a N_2 molecule on the $Ti_3C_2O_2$ slab surface was calculated according to the formula

$$E_{ads} = E_{slab+N_2} - E_{slab} - E_{N_2} \quad (4)$$

where E_{slab+N_2} and E_{slab} are the total energy of the $Ti_3C_2O_2$ supercell with and without an adsorbed N_2 molecule, and $E_{N_2}$is the total energy of a free N_2 gas molecule. Under this definition, a negative adsorption energy indicates that the N_2 molecule can be adsorbed on the $Ti_3C_2O_2$ surface stably. A more negative E_{ads} signifies the stronger adsorption of the N_2 molecule.

A 5 × 5 × 1 $Ti_3C_2O_2$ supercell was built to study the adsorption property of N_2. In addition, Ti atoms with different O coordination environment were set to simulate the chemical activity of the different valance states of $Ti^{(4-x)+}$. Specifically, some O atoms on one side of the $Ti_3C_2O_2$ layer were removed, leaving the underlying Ti atoms exposed. The exposed Ti atoms were bonded with O atoms in different numbers. As shown in Figure 6f,g, the Ti1 site represents a Ti atom without bonding to any O atoms, the Ti2 site denotes a Ti atom bonding to only one O atom, the Ti3 and Ti4 sites refer to Ti atoms bonding to two and three O atoms, respectively. In order to find the optimal configuration of N_2 on the $Ti_3C_2O_2$ surface, a number of possible positions and orientations were considered. During the searching process, a free N_2 molecule was initially placed on the surface randomly. Such placement can provide sufficient initial guess for the most stable adsorbed configuration. Due to the attractive force between the adsorbent and the

adsorbate, the N_2 molecule would be adsorbed onto the surface of $Ti_3C_2O_2$ after structural relaxation.

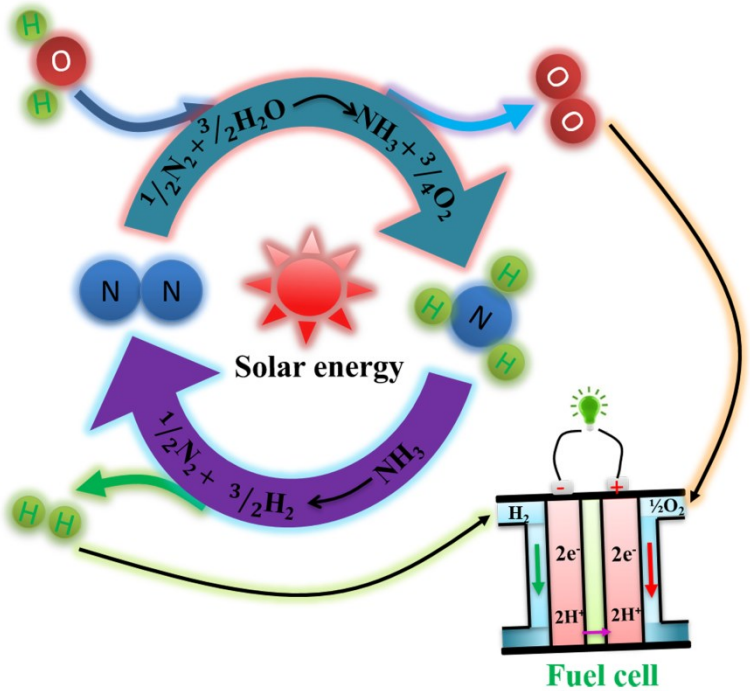

Fig. S1 Schematic illustrating the N_2/NH_3 cycle.

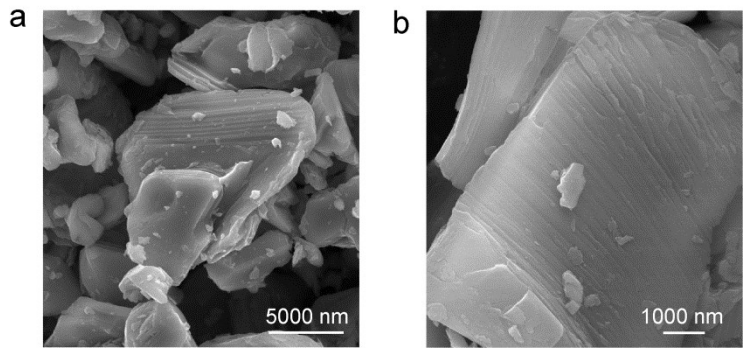

Fig. S2 SEM images of Ti_3AlC_2. (a) Low magnification. (b) High magnification.

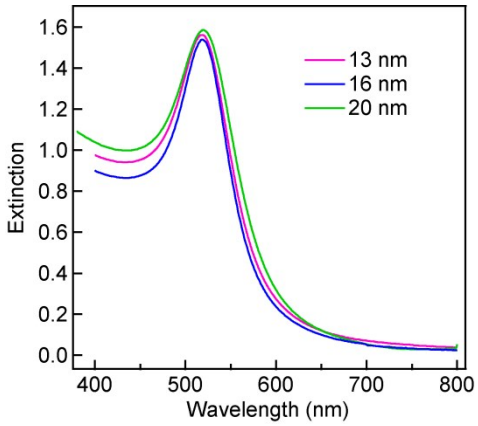

Fig. S3 Extinction spectra of the differently sized Au nanospheres in water.

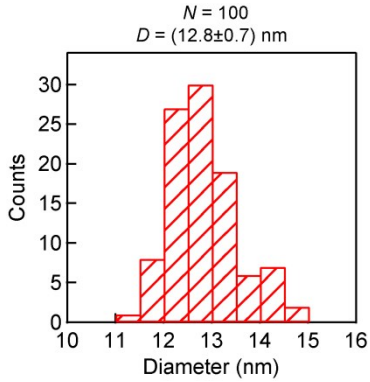

Fig. S4 Histogram of the size distribution of the 13 nm Au nanospheres.

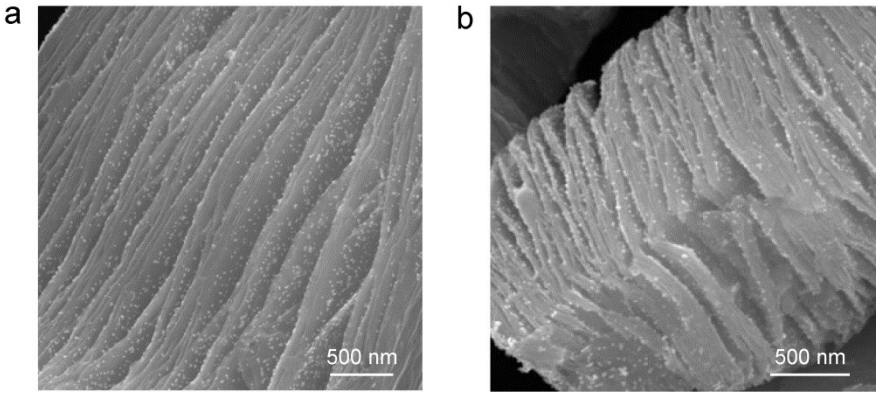

Fig. S5 Low-magnification SEM images. (a) Ti_3C_2/Au. (b) r-Ti_3C_2/Au.

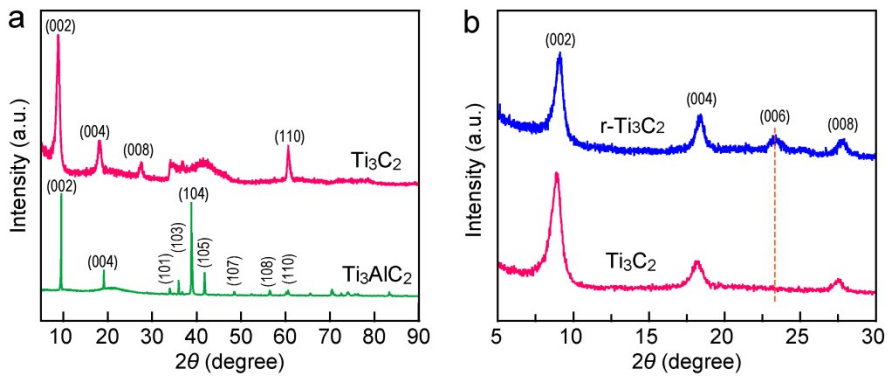

Fig. S6 XRD characterization. (a) Patterns of the Ti_3AlC_2 and Ti_3C_2 samples. (b) Magnified patterns in the region of 2θ = 5–30°.

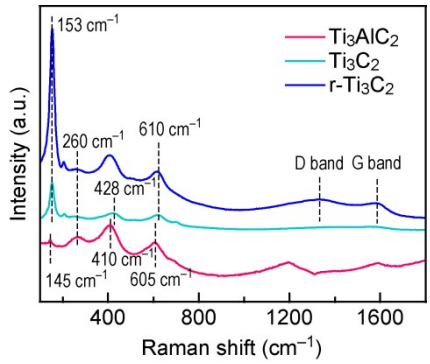

Fig. S7 Raman spectra of Ti_3AlC_2, Ti_3C_2 and r-Ti_3C_2.

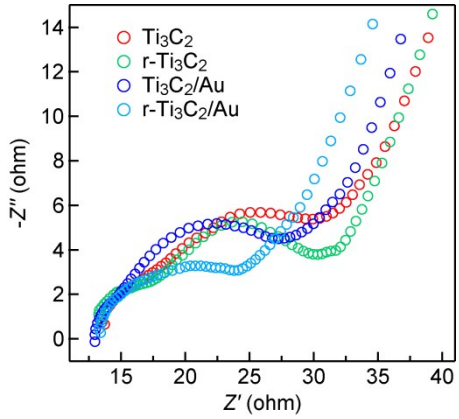

Fig. S8 Nyquist plots of Ti_3C_2, r-Ti_3C_2, Ti_3C_2/Au and r-Ti_3C_2/Au in N_2 under white light illumination.

Fig. S9 Photograph of the photocatalytic N_2 fixation reactor.

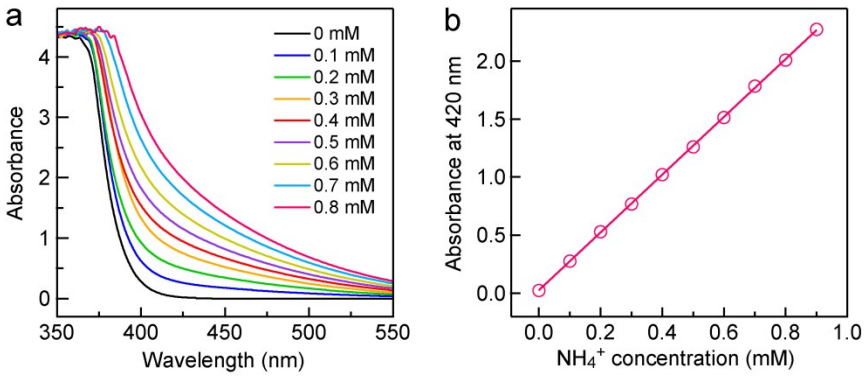

Fig. S10 Dependence of the absorbance on the NH_4^+ determination. (a) Absorption spectra of the standard NH_4^+ solutions at different concentrations. (b) Linear relationship between the absorbance at 420 nm and the NH_4^+ concentration ($y = 0.026x + 2.4887$, $R^2 = 0.9999$).

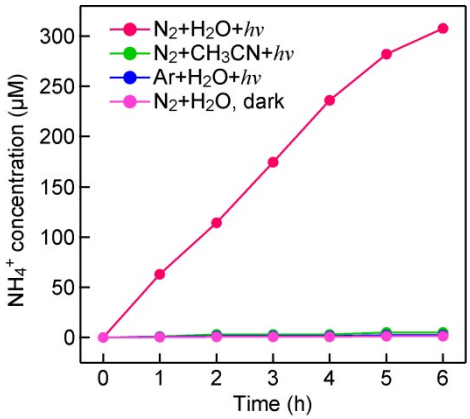

Fig. S11 Control experiments on the photocatalytic N_2 fixation with r-Ti_3C_2/Au under different reaction conditions and white light illumination.

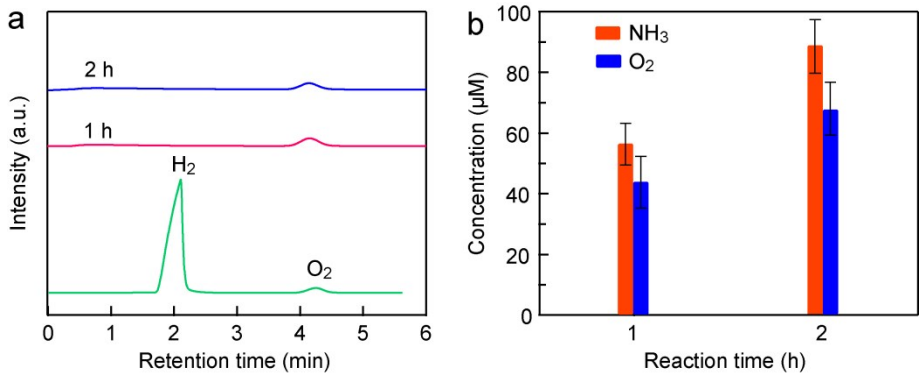

Fig. S12 Analysis of the products of the photocatalytic N_2 fixation reaction with r-Ti_3C_2/Au. (a) Gas chromatograph of the photocatalytic N_2 fixation reaction solution under white light illumination for 1 and 2 h in a sealed system. The green line shows the H_2 and O_2 standards. (b) Amounts of NH_3 and O_2 after the reaction for 1 and 2 h in a sealed system.

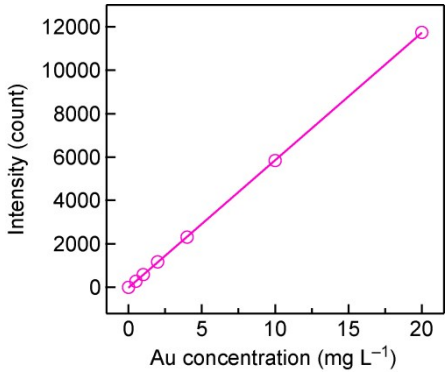

Fig. S13 Linear relationship between the intensity and the standard Au concentration (y = 587.09x–13.32, R^2 = 0.9999).

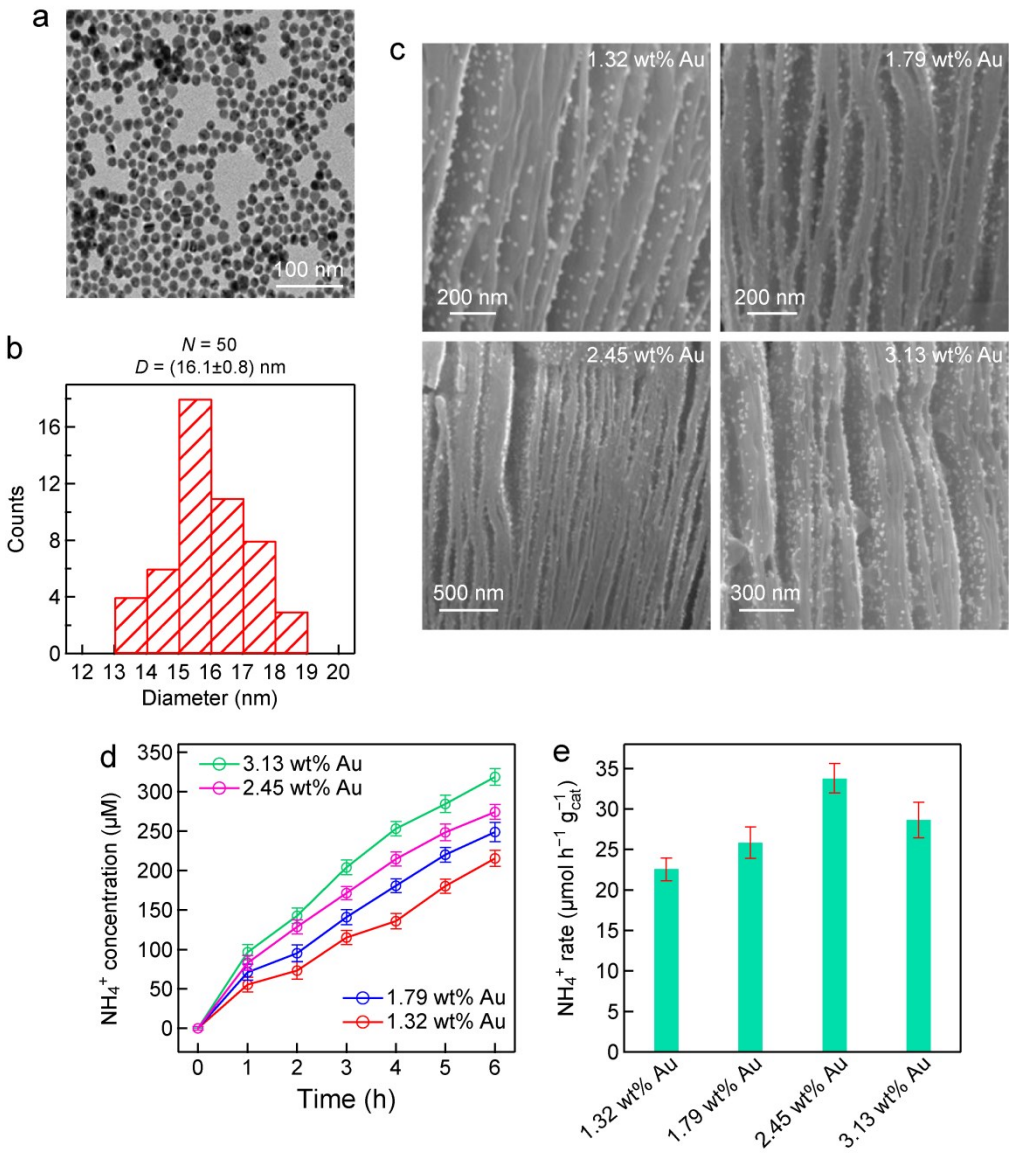

Fig. S14 Characterization and N_2 photofixation activity of the r-Ti_3C_2/Au samples containing the 16-nm Au nanospheres. (a) TEM image of the Au nanospheres. (b) Histogram of the diameter distribution of the Au nanospheres. (c) SEM images of the r-Ti_3C_2/Au samples with the loaded Au amounts indicated in the images. (d) Time courses of the NH_3 concentrations over the r-Ti_3C_2/Au samples with the different Au amounts under white light. (e) NH_3 production rates over the r-Ti_3C_2/Au samples with the different Au amounts under white light.

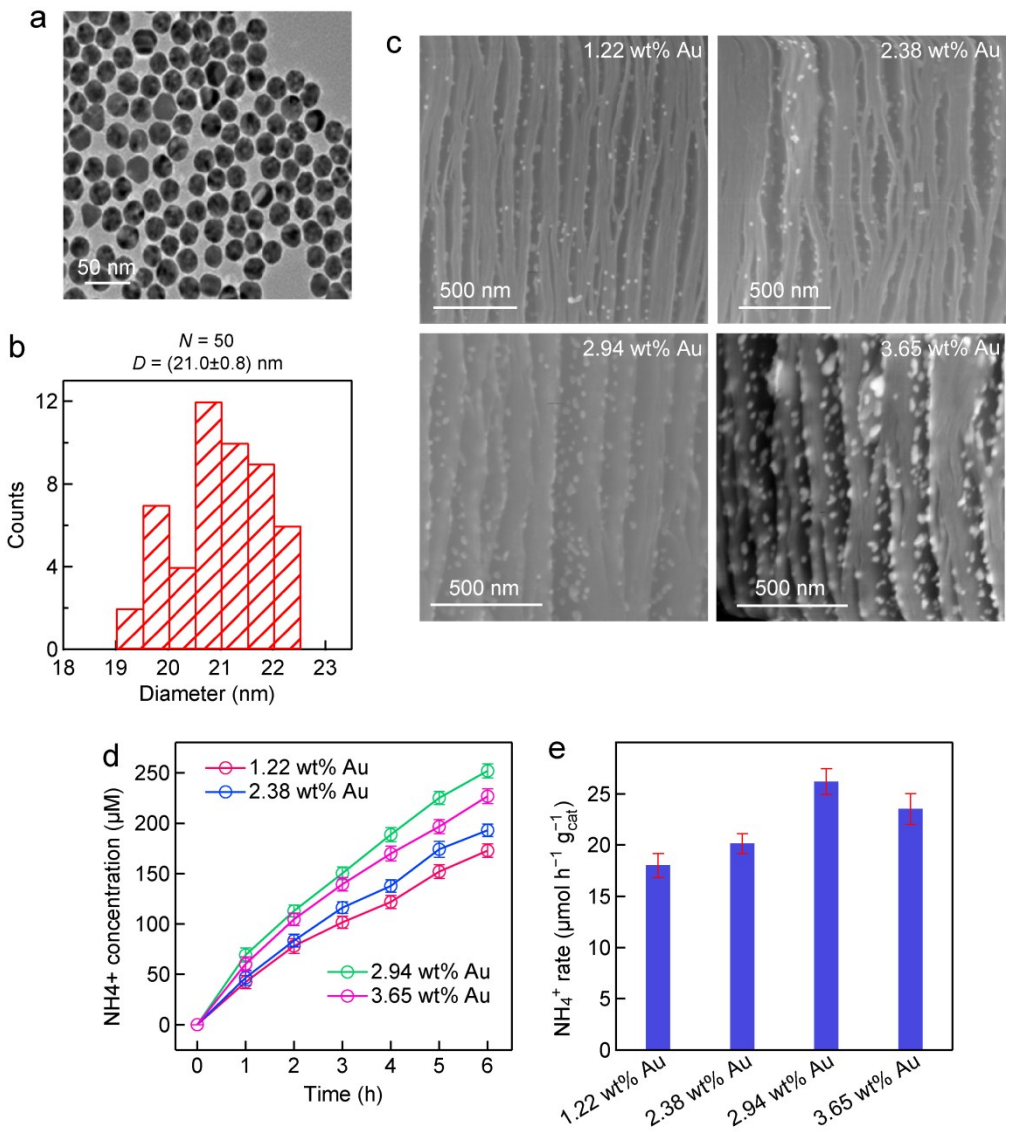

Fig. S15 Characterization and N_2 photofixation activity of the r-Ti_3C_2/Au samples containing the 20-nm Au nanospheres. (a) TEM image of the Au nanospheres. (b) Histogram of the diameter distribution of the Au nanospheres. (c) SEM images of the r-Ti_3C_2/Au samples with the loaded Au amounts indicated in the images. (d) Time courses of the ammonia concentrations over the r-Ti_3C_2/Au samples with the different Au amounts under white light. (e) NH_3 production rates over the r-Ti_3C_2/Au samples with the different Au amounts under white light.

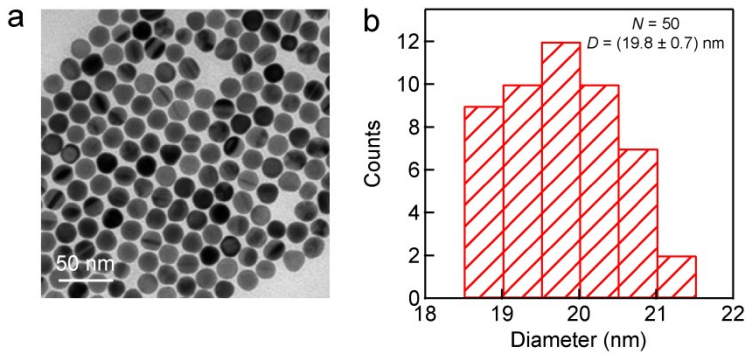

Fig. S16 CTAB-capped 20-nm-sized Au nanospheres. (a) TEM image of the Au nanospheres. (b) Histogram of the diameter distribution of the Au nanospheres.

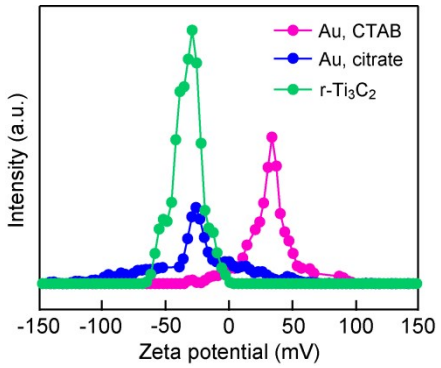

Fig. S17 Zeta potential measurements. The Zeta potentials of the citrate-capped, CTAB-capped 20-nm-sized Au nanospheres and the r-Ti_3C_2 sample dispersed in water.

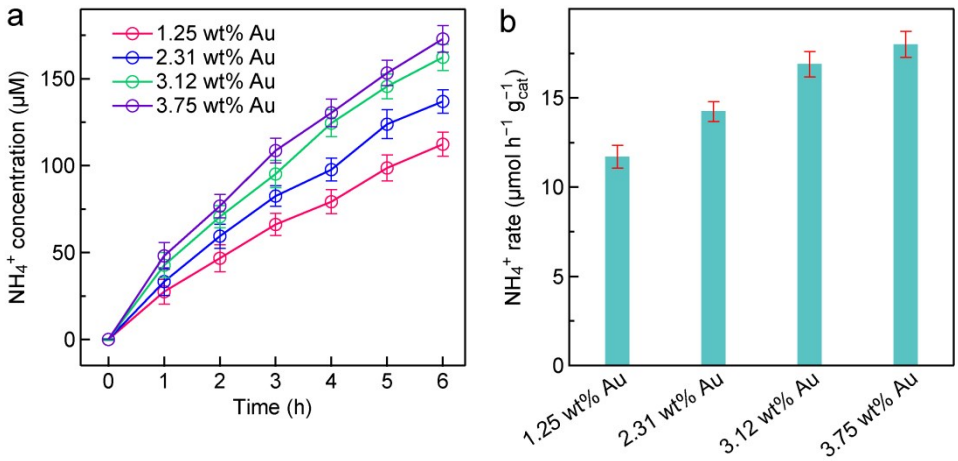

Fig. S18 Photocatalytic N_2 fixation over r-Ti_3C_2/edge-Au with different loaded Au amounts under white light illumination. (a) Time courses of the NH_3 concentrations. (b) NH_3 production rates.

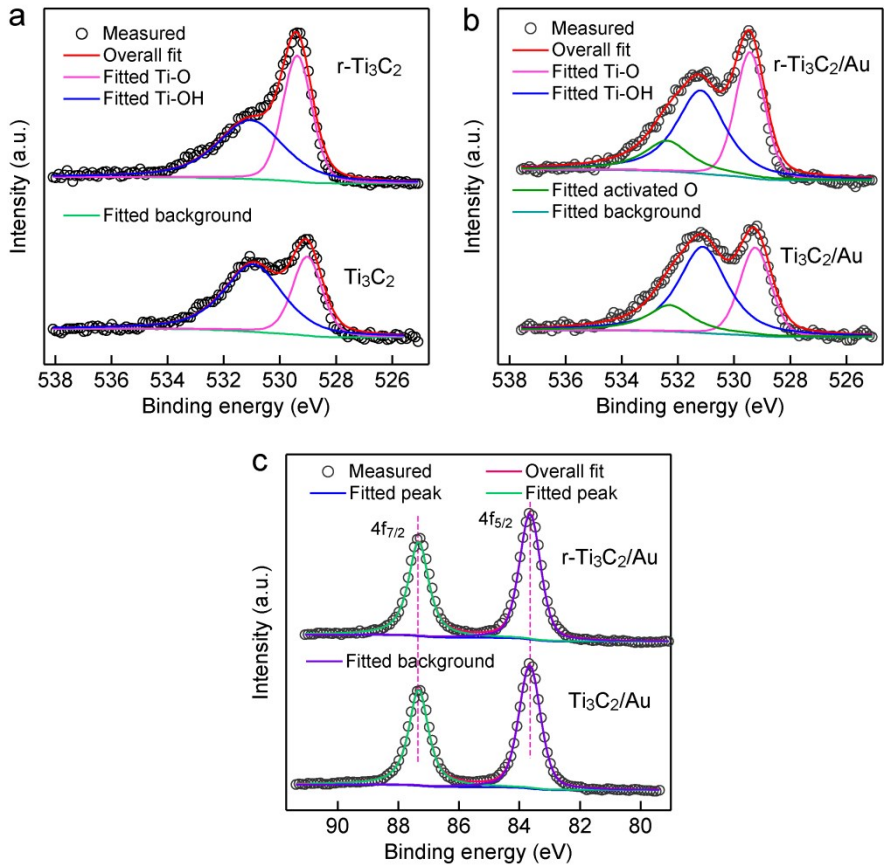

Fig. S19 XPS analysis. (a) High-resolution O 1*s* spectra of the Ti_3C_2 and r-Ti_3C_2 samples. (b) High-resolution O 1*s* spectra of the Ti_3C_2/Au and r-Ti_3C_2/Au samples. (c) High-resolution Au 4*f* spectra of the Ti_3C_2/Au and r-Ti_3C_2/Au samples.

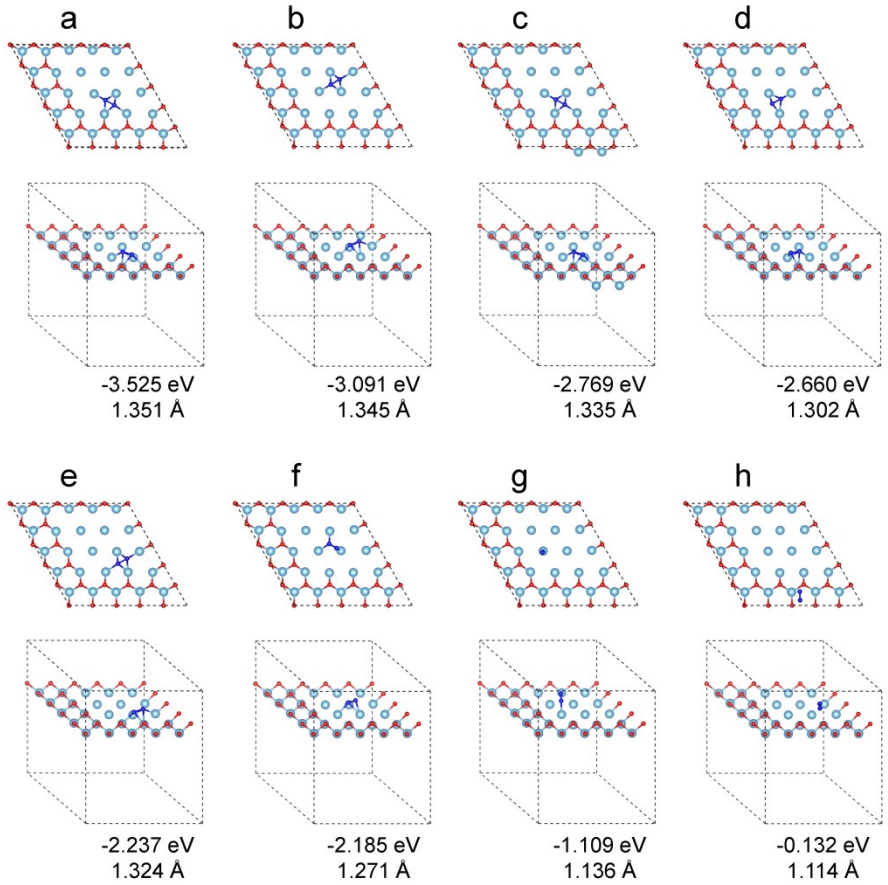

Fig. S20 Configurations of a N_2 molecule adsorbed at the different Ti sites on the surface of r-Ti_3C_2. Light blue balls: Ti; red balls: O; dark blue balls: N. The top and bottom rows are the views along different angles.

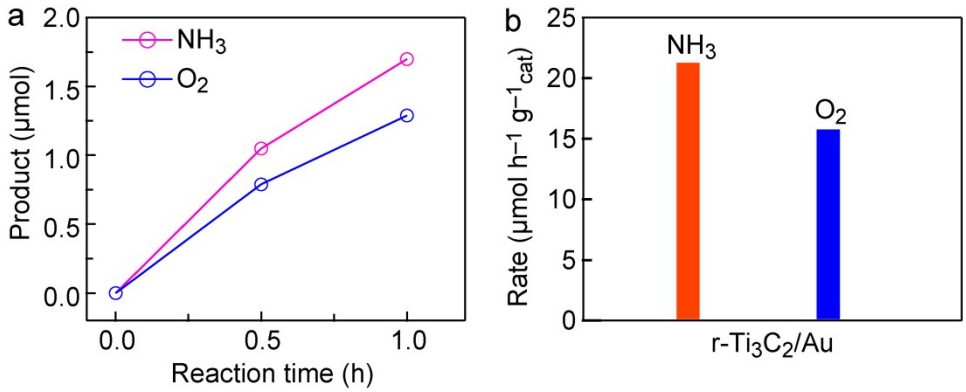

Fig. S21 N_2 photofixation reaction performed under AM 1.5G light illumination. (a) Amounts of NH_3 and O_2 formed in a sealed system. (b) NH_3 and O_2 production rates in the sealed system.

Table S1 Ratios of the Ti atoms in the different valence states in Ti_3C_2 and r-Ti_3C_2 analyzed by XPS

Sample	Ti valence state		
	Ti^{2+} (%)	Ti^{3+} (%)	Ti^{4+} (%)
Ti_3C_2	32.65	18.21	49.14
r-Ti_3C_2	40.86	36.18	22.96

Table S2 Calculated AQEs for NH_3 generation at different wavelengths

Wavelength (nm)	NH_3 produced (μmol h^{-1})	Light power density (mW cm^{-2})	Light power (mW)	AQE (%)
380	1.85	3.26	80.26	0.419
420	2.20	3.48	85.68	0.467
450	2.52	3.56	87.65	0.521
475	3.05	3.69	90.85	0.610
500	3.34	3.72	91.59	0.663
520	3.55	3.76	92.57	0.697
550	3.20	3.78	93.06	0.679
578	3.23	3.81	93.80	0.625
600	2.94	3.86	95.03	0.563
650	2.72	3.89	95.77	0.515
700	2.34	3.72	91.59	0.463

The reactor was illuminated with light from top. The projected area of the reactor in the direction of the light illumination was circular with a diameter of 5.6 cm. The illumination area, *S*, of the solution is therefore

$$S = \pi \times (\frac{d}{2})^2 = \pi \times (\frac{5.6}{2})^2 = 24.62\ cm^2 \quad (5)$$

Take the determination of the AQE at 520 nm as an example. The light power is

$$P = IS = 3.76 \times 24.62 = 92.57\ mW \quad (6)$$

The number of incident photons is

$$N_{\text{incident}} = \frac{Pt}{hv} = \frac{Pt\lambda}{hc} = \frac{92.57 \times 10^{-3} \times 3600 \times 550 \times 10^{-9}}{6.63 \times 10^{-34} \times 3 \times 10^{8}} = 9.21 \times 10^{20}$$

(7)

In the equation above, P is the light power, t is the illumination time (1 h = 3600 s), h is Planck's constant, v is the light frequency, and c is the speed of light in free space. The number of reacted electrons is

$$N_{\text{reacted}} = 3 \times \text{number of the generated } NH_3 \text{ molecules} \quad (8)$$

$$= 3 \times 3.55 \times 10^{-6} \times 6.02 \times 10^{23} = 6.42 \times 10^{18}$$

The AQE can then be calculated as

$$\text{AQE} = \frac{N_{\text{reacted}}}{N_{\text{incident}}} \times 100\% = \frac{6.42 \times 10^{18}}{9.21 \times 10^{20}} \times 100\% = 0.697\% \quad (9)$$

Table S3 AQEs for N_2 photofixation in recent works

Photocatalyst	AQE	Reference
Au/hollow mesoporous C_3N_4 spheres with NVs	0.64% at 550 nm	6
BiOBr with OVs	0.23% at 420 nm	7
$AgInS_2/Ti_3C_2$ Z-scheme heterojunction	0.07% at 420 nm	8
Cu-doped TiO_2	0.23% at 420 nm	9
WO_3 with OVs calcined at 600 ^oC	0.13% at 420 nm	10
Porous $Cu_{96}Fe_4$	0.13% at 535 nm	11
Nitrogen defective C_3N_4/BiO quantum dots	0.53% at 400 nm	12
$Ti_3C_2T_x/TiO_2$ calcined at 400 ^oC	0.05% at 630 nm, 0.07% at 740 nm	13
Fe single atom/triphenylphosphine/NaI	0.05% at 490 nm	14
Bi_2WO_6 with OVs	0.04% at 420 nm	15
MoO_{3-x} nanosheets	0.31% at 808 nm	16
F-doped TiO_2 with OVs	0.38% at 420 nm	17
r-Ti_3C_2/Au	0.697% at 520 nm	this work

AQE, apparent quantum efficiency; NVs, nitrogen vacancies; OVs, oxygen vacancies.

References

1 M. Naguib, M. Kurtoglu, V. Presser, J. Lu, J. J. Niu, M. Heon, L. Hultman and Y. Gogotsi, *Adv. Mater.*, 2011*,* **23***,* 4248.

2 X. H. Ji, X. N. Song, J. Li, Y. B. Bai, W. S. Yang and X. G. Peng, *J. Am. Chem. Soc.*, 2007*,* **129***,* 13939.

3 Q. F. Ruan, L. Shao, Y. W. Shu, J. F. Wang and H. K. Wu, *Adv. Opt. Mater.*, 2014*,* **2***,* 65.

4 Y. X. Zhao, R. Shi, X. A. Bian, C. Zhou, Y. F. Zhao, S. Zhang, F. Wu, G. I. N. Waterhouse, L. Z. Wu, C. H. Tung and T. R. Zhang, *Adv. Sci.*, 2019, **6**, 1802109.

5 S. Grimmw, J. Antony, S. Ehrlich and H. Krieg, *J. Chem. Phys.*, **2010**, *132*, 154104.

6 Y. Z. Guo, J. H. Yang, D. H. Wu, H. Y. Bai, Z. Yang, J. F. Wang and B. C. Yang, *J. Mater. Chem. A*, 2020, **8**, 16218.

7 X. L. Xue, R. P. Chen, H. W. Chen, Y. Hu, Q. Q. Ding, Z. Liu, L. B. Ma, G. Y. Zhu, W. J. Zhang, Q. Yu, J. Liu, J. Ma and Z. Jin, *Nano Lett.*, 2018, **18**, 7372.

8 J. Z. Qin, X. Hu, X. Y. Li, Z. F. Yin, B. J. Liu and K. Lam, *Nano Energy*, 2019, **61**, 27.

9 Y. X. Zhao, Y. F. Zhao, R. Shi, B. Wang, G. I. N. Waterhouse, L. Z. Wu, C. H. Tung and T. R. Zhang, *Adv. Mater.*, 2019, **31**, 1806482.

10 T. T. Hou, Y. Xiao, P. X. Cui, Y. N. Huang, X. P. Tan, X. S. Zheng, Y. Zou, C. X. Liu, W. K. Zhu, S. Q. Liang and L. B. Wang, *Adv. Energy Mater.*, 2019, **9**, 1902319.

11 T. T. Hou, L. L. Chen, Y. Xin, W. K. Zhu, C. Y. Zhang, W. H. Zhang, S. Q. Liang and L. B. Wang, *ACS Energy Lett.*, 2020, **5**, 2444.

12 C. Liang, H. Y. Niu, H. Guo, C. G. Niu, Y. Y. Yang, H. Y. Liu, W. W. Tang and H. P. Feng, *Chem. Eng. J.*, 2021, **406**, 12868.

13 T. T. Hou, Q. Li, Y. D. Zhang, W. K. Zhu, K. F. Yu, S. M. Wang, Q. Xu, S. Q. Liang and L. B. Wang, *Appl. Catal. B: Environ.*, 2020, **273**, 119072.

14 T. T. Hou, H. L. Peng, Y. Xin, S. M. Wang, W. K. Zhu, L. L. Chen, Y. Yao, W. H. Zhang, S. Q. Liang and L. B. Wang, *ACS Catal.*, 2020, 10, 5502.

15 T. Y. Wang, C. T. Feng, J. Q. Liu, D. J. Wang, H. M. Hu, J. Hu, Z. Chen and G. L. Xue, *Chem. Eng. J.*, 2021, **414**, 128827.

16 H. Y. Wu, X. Li, Y. Cheng, Y. H. Xiao, R. F. Li, Q. P. Wu, H. Lin, J. Xu, G. Q. Wang, C. Lin, X. Y. Chen and Y. S. Wang, *J. Mater. Chem. A*, 2020, **8**, 2827.

17 R. Q. Guan, D. D. Wang, Y. J. Zhang, C. Liu, W. Xu, J. O. Wang, Z. Zhao, M. Feng, Q. K. Shang and Z. C. Sun, *Appl. Catal. B: Environ.*, 2021, **282**, 119580.